

YIMIN SONG<sup>1</sup>\*, HE REN<sup>1</sup>, HAILIANG XU<sup>1</sup>, DONG AN<sup>1</sup>**EXPERIMENTAL STUDY ON DEFORMATION AND DAMAGE EVOLUTION  
OF A MINING ROADWAY WITH WEAK LAYER ROCK  
UNDER COMPRESSION-SHEAR LOAD**

The structure and load characteristics of the roadway are simplified, and the experimental model of the roadway deformation and damage under compression-shear load is established. The experimental data acquisition system is built with a CCD camera. The digital speckle correlation method is used to calculate the image data of the experimental model. The correspondence between the evolution law of the deformation field, the interlayer displacement and deformation evolution are analysed, including the dynamic characteristic of the roadway surrounding the rock. Research results indicate: (1) The damage peak load of the weak layer structure shows a decreasing trend as the interlayer shear stress increases. As the initially applied shear stress increases, the value of interlayer sliding displacement increases, and the dynamic characteristics become more apparent. (2) In the sub-instability phase of the loading curve, when the surrounding rock slides along the layers under compression-shear load, the stress is re-distributed and transmitted to the deep part of the surrounding rock. Then the surrounding rock of the roadway forms the characteristic of alternating change, between tension to compression. (3) According to the state of dynamic and static mechanics, the deformation evolution of the roadway before the peak load belongs to the static process. Zonal fracturing is part of the transition phase from the static process to the slow dynamic process, and the rockburst damage is a high-speed dynamic process. (4) Under the compression-shear load, due to the weak layer structure of the coal and rock mass, the local fracture, damage, instability and sliding of the surrounding rock of the roadway are the mechanical causes of rockburst. (5) Even if the coal and rock mass does not have the condition of impact tendency, under stress load of the horizontal direction, distribution of large shear stress is formed between layers, and the dynamic damage of the rockburst may occur.

**Keywords:** rock burst, zonal fracturing, compression-shear load, interlayer displacement, Digital Speckle Correlation method

<sup>1</sup> NORTH CHINA UNIVERSITY OF TECHNOLOGY, SCHOOL OF CIVIL ENGINEERING, CHINA

\* Corresponding author: [ssyymmok@sina.com](mailto:ssyymmok@sina.com)



© 2021. The Author(s). This is an open-access article distributed under the terms of the Creative Commons Attribution-NonCommercial License (CC BY-NC 4.0, <https://creativecommons.org/licenses/by-nc/4.0/deed.en>) which permits the use, redistribution of the material in any medium or format, transforming and building upon the material, provided that the article is properly cited, the use is non-commercial, and no modifications or adaptations are made.

## 1. Introduction

Mining roadway is one of the most important structures in mining engineering, whose deformation and damage affect the safety in mine production directly. In recent years, with the increase of mining depth, not only the accidents of rockburst in roadway become more frequent [4,9,6,19], but also the phenomenon of zonal fracturing in surrounding rock of roadway is different from shallow mining. Rock burst and zonal fracturing in the roadway are two focused issues in mining engineering at present. Scholars have studied the two engineering phenomena from different angles and made many meaningful research achievements. From the essence of engineering, rock burst and zonal fracturing in the roadway are two typical deformations and damaged states of the roadway in mining engineering. Therefore, it is of great significance to study the evolution characteristics of roadway deformation and damage. It is beneficial to reveal the mechanism of roadway-related engineering phenomena and disasters, and it has important theoretical and practical value for mining engineering.

According to the analysis of relevant articles, there are similarities in structure and load characteristics in the occurrence of rockburst and zonal fracturing of mining roadway. From the structural characteristics, the roadway corresponding to the two deformation and damage states are in the weak structure of the stratified rock mass. Secondly, from the load characteristics, the horizontal stress is large, that is, the interlayer shear force exists. Based on the above understanding of the characteristics, scholars have carried out useful explorations and attempts from the friction and sliding effect between layers. Shemyakin et al. [10-13] discovered the zonal fracture phenomenon by using a resistivity meter at the mining site of Taimyrskii. Kurlenya et al. [3] discovered the irregular ultra-low friction phenomenon of rock mass in the study of dynamic propagation of deep block rock mass and conducted relevant experimental research. Pan [18] aims at the obvious dislocation phenomenon of coal and rock mass when deep rock bursts occur and studies the occurrence law of ultra-low friction of block rock mass based on pendulum-type wave propagation theory. Qi [7,8] thinks that the process of rockburst is the instantaneous stick-slip process of coal and rock strata, and it is the dynamic process that coal and rock strata meet the shear strength criterion to slide suddenly with the release of kinetic energy in the sliding process. The weak structural plane and layered interface, which is easy to slide abruptly, are the most important factors leading to rockburst. Li [5] deduced a new formula of normal force between blocks and a new formula of horizontal displacement of working blocks by establishing a theoretical model of ultra-low friction effect of block rock mass considering overburden pressure. The research shows that the decrease of normal force between blocks leads to the decrease of friction between blocks, and in the case of horizontal disturbance, it is easy to induce ultra-low friction rockburst. Li [2] restored the restraint effect of roof and floor on coal seam through the clamping test of designed displacement control. The research shows that the locking effect of roof and floor on coal seam and the deformation conduction of coal seam itself can promote the formation of rockburst. According to the concept of structural instability, Lippman [1] thinks that when the static coal seam is disturbed, it causes relative sliding between the coal seam, the roof and floor, and a slight displacement to the roadway. After the bearing capacity of the coal seam reaches its limit, this disturbance may cause a coal seam outburst, otherwise, it will be a purely static response. In the study of zonal fracturing, The measurement results of alternating tension and compression deformation zones in surrounding rock are obtained by Fang [20] according to the on-site monitoring of surrounding rock in the roadway in bad rock strata. Zhang [15] carried out the true 3D loading geomechanics model test of the layered jointed rock mass with weak

interlayer by using a model similar in material and high-geostress true 3D loading geomechanics model test system. The research shows that the weak interlayer is an important factor affecting the zonal fracturing phenomenon of the layered jointed rock mass. Taking the deep roadway with high geostress in the Dingji Coal Mine of Huainan Mining Area as the prototype, Xu [16], et al. carried out a three-dimensional similar model test of blasting excavation of deep surrounding rock under the condition of high-axis geostress. The results show that explosion load produces a large number of microcracks near the roadway wall, which leads to the deterioration of its mechanical properties and the decrease of its integrity. At the same time, the geostress is adjusted. The radial tensile strain of the vault, sidewall and bottom plate changes with the distance from the roadway wall increasing, showing wave changes with peaks and valleys distributed at intervals. Although a great deal of work has been done in the above-mentioned research fields and some meaningful results have been obtained, there are still some deficiencies in the research on some of the basic problems in the evolution characteristics of roadway deformation and damage caused by interlaminar compression-shear loads. There is still a lack of in-depth and meticulous research on the evolution law of the roadway deformation field, the evolution characteristics of interlayer friction, sliding, the dynamic characteristics of roadway deformation and damage in different loading stages. Consequently, the evolution process of deformation and damage of the roadway in weak rock mass under compression-shear load is observed by an experimental method. It is hoped that the preliminary research work in this paper will play a role in attracting valuable investment and provide an experimental reference for further exploring the mechanism and process of rockburst and zonal fracturing.

In this paper, an experimental model of roadway deformation and damage under compression-shear load is established according to the similarity of structure and load characteristics between rockburst and zonal fracturing. A CCD camera is used to set up the experimental data acquisition system and for calculating the image data of the experimental model through the Digital Speckle Correlation method. The evolution law of the deformation field of weak layer rock, the corresponding relationship between shear strain and normal strain evolution of weak layer rock and interlayer friction and sliding, and the dynamic characteristics of weak layer rock deformation and evolution are analysed. Finally, the combination of experimental analysis, the occurrence mechanism of two kinds of roadway deformations, the damage states, including zonal fracturing and roadway rockburst will be discussed.

## 2. Experiment

### 2.1. Experimental model design and monitoring scheme

The mechanical model of a roadway in mining engineering is shown in Fig. 1(a), in which the boundary conditions of the model are normal stress  $\sigma_x$  in the horizontal direction and normal stress  $\sigma_y$  in the vertical direction. When there are different physical and mechanical conditions of rocks in different strata, the free surface formed by roadway excavation, load in horizontal and vertical directions  $\sigma_x \neq \sigma_y$ , etc., the rock strata in which the roadway is located will be under compression-shear stress. Micro-segments are selected to build micro-elements in the rock stratum where the roadway is located, and its schematic diagram of force is shown in Fig. 1(b).

The experimental model consists of three rocks, which represent the roof, the floor rock mass and weak rock mass, respectively. Among them is a granite material used to simulate the

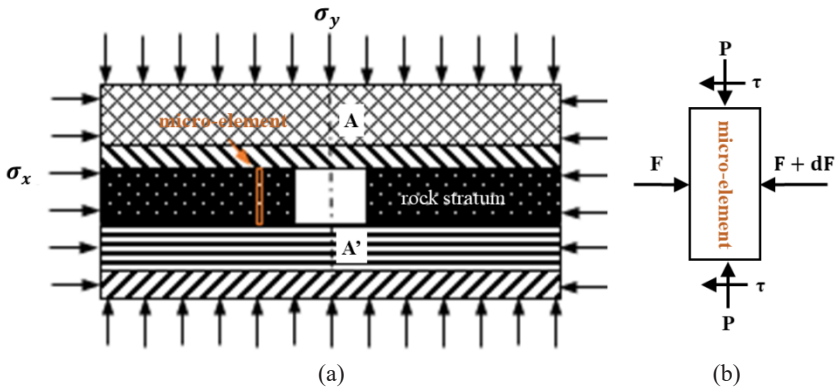


Fig. 1. Mechanical model of roadway in mining engineering

roof and floor rock mass of the model. Red sandstone material is used to simulate the weak rock mass of the model roadway. The elastic modulus of granite is 63.7 GPa, and Poisson’s ratio is 0.27. The elastic modulus of red sandstone is 34.3 GPa, and Poisson’s ratio is 0.32. The size of the top and bottom floor of the model is 300×100×50 mm, while the weak floor of the model is 270×50×50 mm. The sliding surface is polished with 300# carborundum paper, and the surface of the specimen is painted to make a speckle field. Model combination, loading boundary conditions, deformation field analysis area and sliding displacement monitoring points are shown in Fig. 2. The model adopts bi-directional loading, in which vertical load is applied in the vertical direction, and transverse load is applied in the horizontal direction. The load is applied step by step according to the experimental scheme. With A-A’ in Fig. 1(a) as the symmetry axis, aligning the top and bottom plates of the design model on the right side and constraining the horizontal

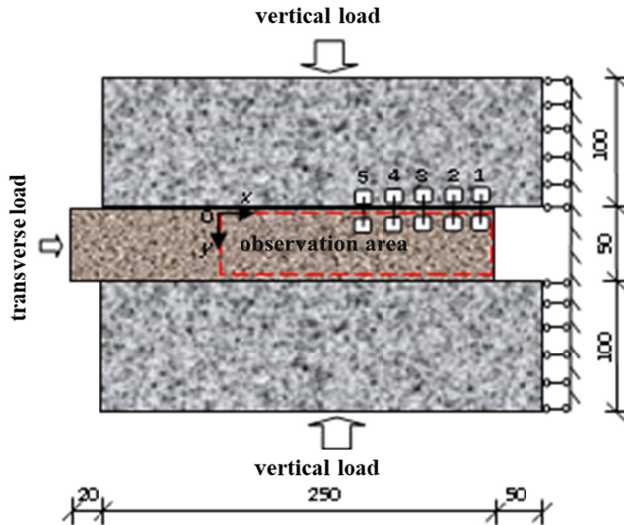


Fig. 2. Diagram of model size and boundary condition (mm)

displacement. On the right side of the weak rock mass, there is a vacant area with a size of  $50 \times 50 \times 50$  mm, which simulates half of the roadway. The observation area in Fig. 2 corresponds to the deformation field evolution analysis area in Sect. 3.1 below. Five pairs of measuring points are selected at equal intervals on the crack interface, and the distance between measuring points is 17mm. Points 1-5 correspond to the measuring points of the evolution characteristics of interlayer sliding velocity and acceleration in Sect. 3.3 below.

## 2.2. Experimental system and experimental method

As shown in Fig. 3, the experimental system consists of a loading system and deformation field observation system based on the Digital Speckle Correlation method.

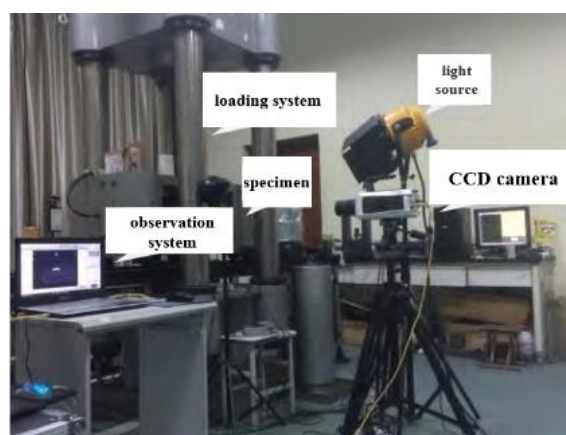


Fig. 3. The sketch of the experimental system

The loading system adopts an RLJW-2000 hydraulic servo testing machine, which can realize bi-directional loading. And loading modes include force control loading and displacement control loading.

Deformation field observation includes image data collection and image data analysis and processing. The acquisition system is built by a CCD camera, and the speckle images of the model surface in the whole loading process from the beginning to the end of the experiment are continuously collected and stored in the computer. The Digital Speckle Correlation method is used to analyse and process the image data. The basic principle is to calculate the displacement field and strain field of the model surface through the correlation identification of the digital gray field based on the assumption that the gray level is unchanged.

The loading of the model is subsection loading, which simulates the evolution law of roadway deformation and damage under the condition of different initial shear stress between layers. The loading process is divided into three stages. In the first stage (Path I), adopting force control loading mode, the vertical load is applied to the model to the preset value and then kept constant. In the second stage (Path II), the force control loading mode is adopted, but the transverse load is applied to the model to a predetermined value to keep the transverse load constant. In the third

stage (Path III), the displacement control loading mode is adopted, and the vertical load is applied to the model until the model is destroyed, then the experiment is finished.

The observation system parameters are: The surface speckle field of rock mass on the top and bottom of the model is its natural speckle field, and the artificial speckle field is formed by spraying black and white glass bead paint on the surface of the weak rock mass. Image acquisition speed of a CCD camera is 5 frames/s, image resolution is 1600×1200 pixel, and object plane resolution is 0.179 mm/pixel. The displacement analysis window of the Digital Speckle Correlation method is set to 31×31 pixel, the analysis step is 5 pixel, and the measurement accuracy is 0.01 pixel.

## 2.3. Experimental process and results

### 2.3.1. Experimental process

Before the experiment, firstly, the loading system and CCD image acquisition system are synchronised to ensure the time synchronisation of the two systems. Then, the models are combined and arranged according to the design size. Finally, debugging the CCD camera and testing machine, and then the preparation for the experiment is finished.

At the start of the experiment, the vertical load was applied to the upper and lower end faces of the specimen by the force control loading method, with a loading rate of 0.435 kN/s. It is essential to stop loading and keep the load constant when the vertical load reaches a predetermined value. Then, the transverse load is applied to the weak rock mass by force control, and the loading rate is 0.435 kN/s. When the load reaches a predetermined value, the load remains unchanged. Finally, the displacement control method is adopted to the load vertically, and the loading rate is 0.25 mm/min until the specimen fails. At the beginning of the experiment, the CCD camera starts to continuously capture speckle images of the specimen surface, and when the model is damaged, the loading and image collection is stopped.

After the experiment, the collected data is organised, and the displacement field and deformation field of the model are calculated by the Digital Speckle Correlation method.

### 2.3.2. Experimental results

Four experiments under different load conditions have been completed. In this paper, the data analysis takes the 4# experimental model as an example, and other experimental results are given in the form of a table. Fig. 4 shows the 4# relationship curve between loading path, load and time. Four groups of experimental loading settings and peak loads are given in Table 1.

TABLE 1

Experimental loading settings and peak loads

Experiment serial number	Path I: vertical load (kN)	Path II: transverse load (kN)	Path III: peak load (kN)
1#	0	0	481.2
2#	50	53	466.3
3#	70	82	420.6
4#	100	115	433.5

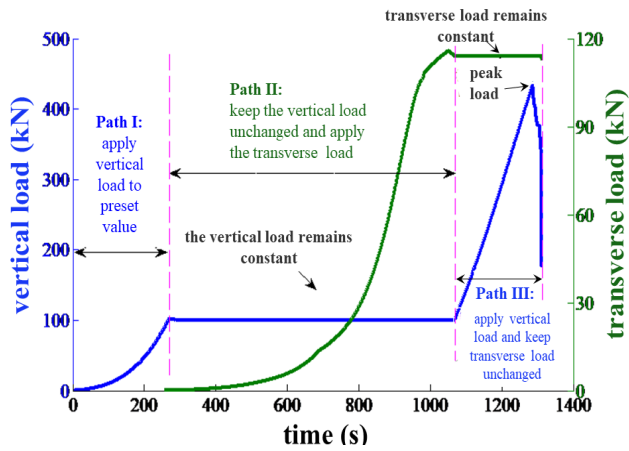


Fig. 4. The 4# relationship curve between loading path, load and time

When different transverse loads are applied to the model, different shear stresses will be produced between the roof and floor of the model, including the layers of the weak rock mass. That is, the greater the lateral load, the greater the interlaminar shear stress. From the above experimental results, the peak load of model damage tends to decrease with the increase of interlayer shear stress.

The surface speckle image at the initial loading time of path III of the 4# experimental model and the fracture damage image of the specimen after the model damage is calculated. Fig. 5 is a comparison of the former two images. It can be seen from Fig. 5 that the damaged area of the model is located at the boundary of the roadway. The damage has the characteristics of suddenness, impact, vibration and the damage range is about 79 mm.

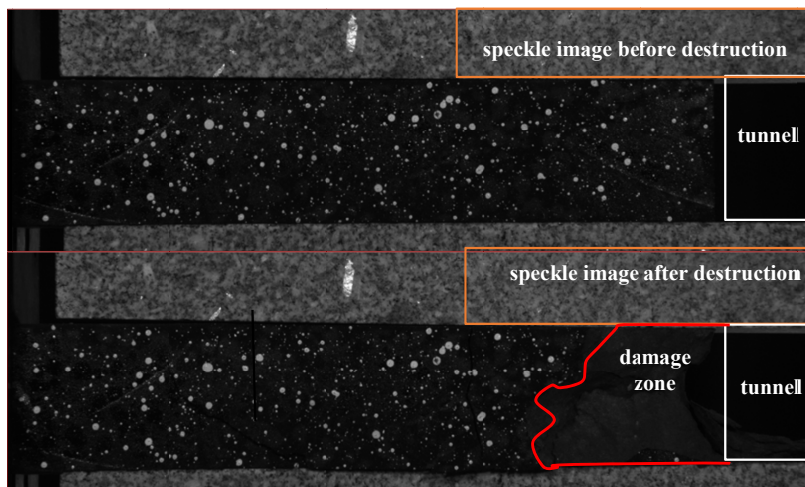


Fig. 5. The damage form of experimental specimen

### 3. Analysis of experimental results

Based on the calculation of displacement field and strain field of speckle images collected from experiments by the Digital Speckle Correlation method, several characteristic indexes of weak rock are analysed. It includes the evolution law of the deformation field, the corresponding relationship between shear strain and normal strain evolution, interlayer friction and sliding, and the dynamic characteristics in the process of deformation evolution. Combined with the experimental analysis results, the mechanism of deformation and damage state of roadway, i.e., zonal fracturing and roadway rockburst, is discussed.

#### 3.1. Study on evolution of deformation field of weak rock

Taking the stage of path III of the 4# experimental model as the research object, according to the characteristics of the vertical load curve, five identification points are selected on the curve. The model surface speckle image acquired at the time corresponding to point 0 is taken as a reference image, and the model surface speckle image acquired at the time corresponding to points 1-4 is taken as a deformed image. Among them, points 1-2 are linear stages of the loading curve, point 3 is the peak time of the loading curve, point 4 is the post-peak stage of the loading curve, the positions and loads of identification points are shown in Fig. 6. The observation area in Fig. 2 is calculated by using the Digital Speckle Correlation method, and the evolution characteristics of the deformation field of weak rock are studied.

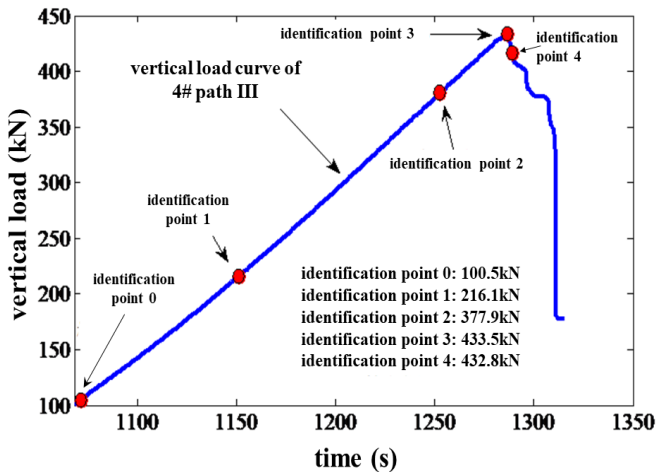


Fig. 6. Vertical load curve of 4# path III

Fig. 7 shows the evolution nephogram of the deformation field (positive strain in  $X$  direction, the same below) of the model at different loading times. In the figure, positive strain indicates that the rock is in tension, while negative strain indicates that the rock is in compression. It can be seen from the figure that the moment when the vertical load is 216.1 kN corresponds to Fig. 7(a). The deformation field in the observation area is in a state of tensile deformation, and the defor-

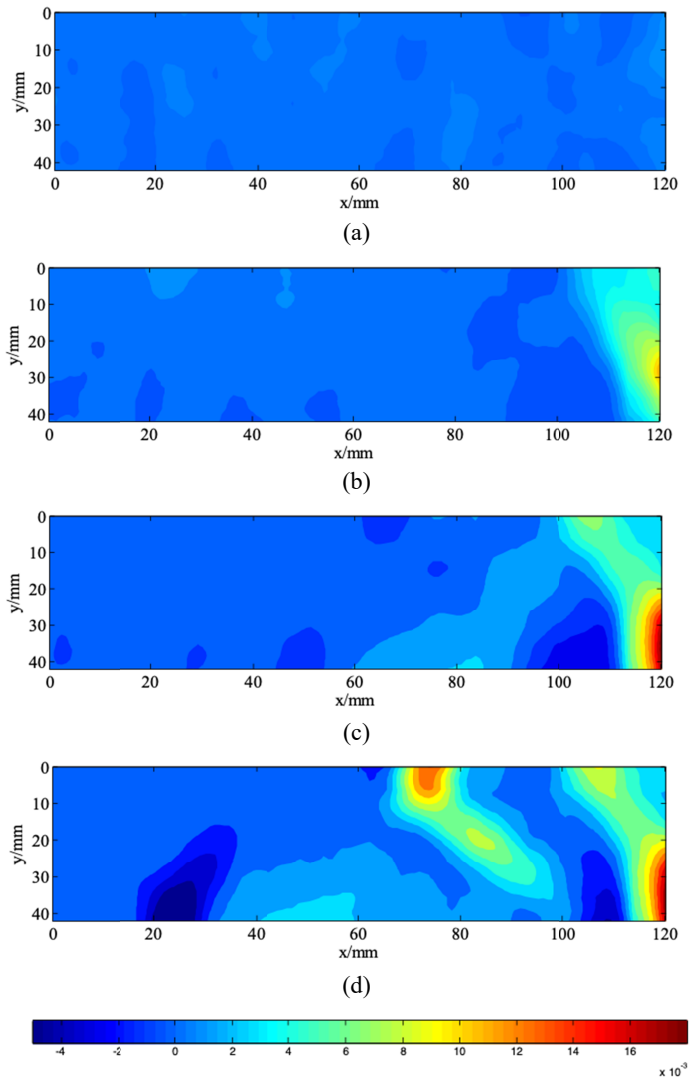


Fig. 7. Evolution of deformation field at different loading moments

mation is evenly distributed with a small magnitude. Fig. 7(b) corresponds to the time when the vertical load is 377.9 kN, and the deformation concentration area appears near the roadway end with the  $x$  coordinate of 105-120 mm, which is in a state of tensile deformation, and the influence range is about 15 mm. Fig. 7(d) is in the post-peak stage of loading, corresponding to the time when the load is 432.8 kN. At the  $x$  coordinate of 65-100 mm, a new concentrated area of tensile deformation occurs. Near the end of the roadway, in the range of  $X$  coordinate 65-120 mm, an obvious tensile-compressive-tensile deformation area is formed. At this moment, it is the last image collected before macroscopic fracture appears in the observation area of the model, and

the whole observation area still keeps a continuous deformation state. At the beginning of the next image acquisition time, macroscopic fracture occurs in the model, and the damaged area appears in the rock stratum. Subsequently, the damaged area breaks further and slides towards the roadway, resulting in dynamic instability.

Through the analysis of the evolution nephogram of the deformation field in the observation area, the following conclusions can be made. There is an uneven distribution of stretching and compression areas alternately near the end of the roadway. With the formation of the damage zone of the model, the macro cracks expand, which will lead to accelerated sliding towards the roadway, resulting in dynamic instability.

### 3.2. Study on the relationship between structural deformation of weak rock and interface friction and sliding

To analyse the deformation process in greater detail, the upper boundary and the centreline is selected in the model. The positions of the line segments are shown in Fig. 8. The  $x$ -direction positive strain value of each point on the centerline segment and the shear strain value of each point on the upper boundary line segment are respectively extracted. Then the curves of normal strain evolution at the centreline and shear strain evolution at the upper boundary at the corresponding time of each identification point are drawn, and the temporal and spatial evolution law of deformation and damage in the observation area is studied.

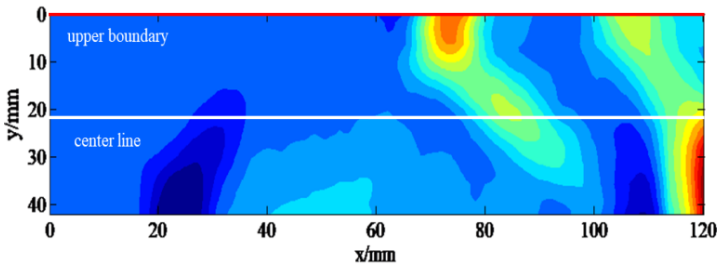


Fig. 8. The location of the upper boundary and centerline

Fig. 9 is the normal strain evolution curve in the  $x$ -direction at different loading times at each point on the centerline segment of the observation area of the weak layer of the model. Among them, the horizontal coordinates are the coordinates of each point of the line segment, and vertical coordinates are the positive variable value of each point. It can be seen from the figure that when the load is carried out to the time corresponding to the identification point 1, the normal strain at each point of the central line segment is evenly distributed and has a small value. The time corresponding to identification point 2, the value of the strain near the roadway in the central line segment increases greatly, resulting in deformation concentration. Compared with identification point 1, other points have no obvious change. At the time of loading to identification point 3, the load reaches its peak. Except for the points near the end of the roadway, the positive strain at other points is transmitted to the end far from the roadway in a fluctuating way, and the value increases. When the load reaches identification point 4, the load is in the post-peak stage. At this

time, two large tensile strain concentration areas are formed at the end of the roadway, and the normal strain presents a large fluctuation distribution as a whole.

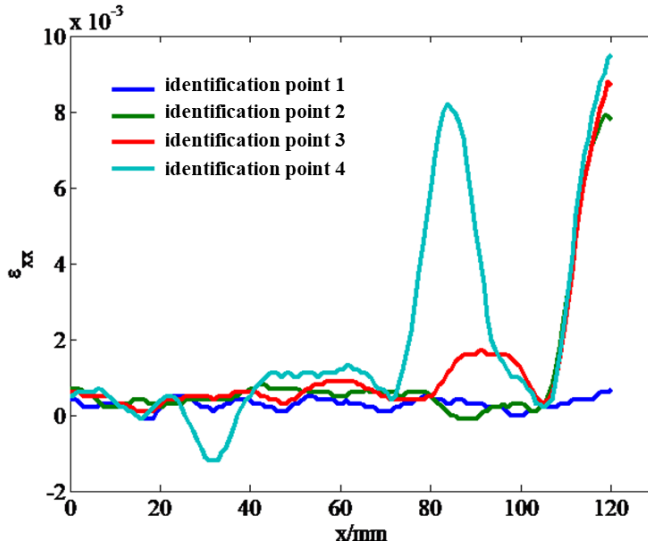


Fig. 9. The evolution curve of  $\varepsilon_{xx}$  at different loading moments

Fig. 10 is the shear strain evolution curve of each point on the boundary line segment in the observation area of the weak layer of the model at different loading times. The horizontal and vertical coordinates represent the coordinates of each point of the line segment and the values of shear strain variables, respectively. As shown in the figure, when loaded to the corresponding time of identification point 1, the shear strain at each point of the upper boundary line segment is relatively uniform, and its magnitude is small. The time corresponding to the identification point 2, the shear strain value in the upper boundary line segment near the end of the roadway increases greatly, and the maximum value of shear strain appears near  $x$  coordinate at a value of 110 mm. Compared with the time associated with identification point 1, the other points of the upper boundary line segment have no obvious change. At the time of loading to identification point 3, the load reaches its peak. Except for the increase of shear strain near the end of the roadway, the shear strain at other points is transmitted to the deep surrounding rock of the roadway in a fluctuating way. At the time of loading to identification point 4, the load is in the post-peak stage, and the shear strain value of the upper boundary line segment fluctuates greatly.

From Fig. 9 and Fig. 10, the evolution trend of normal strain and interlayer shear strain of weak rock is in good agreement. That is to say, the frictional sliding property of the interlayer interface directly affects the deformation and damage evolution process of the weak rock. Therefore, further research on the deformation and damage of the weak rock and their relationship is carried out from the perspective of interlayer friction and slip evolution.

Using the monitoring points shown in Fig. 2, the interlayer sliding displacement is analysed by a virtual extensometer [14]. Fig. 11 shows the evolution curves of sliding displacement of five monitoring points in the whole loading process. The loading curve can be divided into three stages,

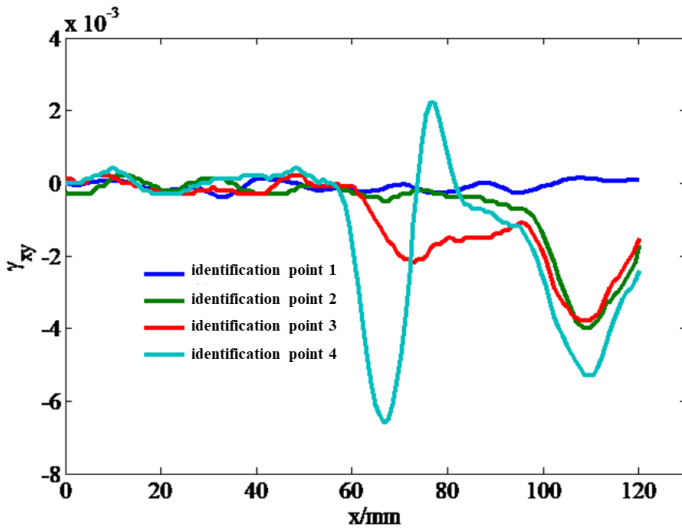


Fig. 10. The evolution curve of  $\gamma_{xy}$  at different loading moments

namely, linear loading stage before peak value, sub-instability stage from peak to rapid decline [17], and instability stage of rapid decline. In the linear loading stage, the sliding displacement of the five monitoring points is small, which is approximately 0. In the stage of sub-instability, the interface between layers corresponding to monitoring points 1-3 slides relatively, the sliding displacement increases rapidly, until it reaches the maximum value, while the interface between layers corresponding to monitoring points 4 and 5 does not slide relatively. In the instability stage, the interlayer interfaces corresponding to monitoring points 1-5 all have relative sliding.

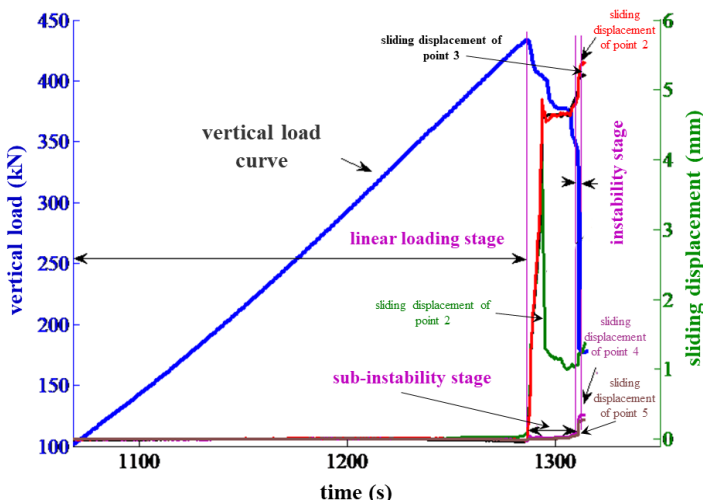


Fig. 11. The evolution curve of interlayer sliding displacement in loading process

Table 2 shows the maximum sliding displacement of each monitoring point in the sub-instability stage of four groups of model experiments. It can be seen from the table that with the increase of initially applied shear stress, the magnitude of sliding displacement increases.

TABLE 2

The maximum displacement values of each measuring point in the experiment

Experiment serial number	Maximum displacement of point 1 (mm)	Maximum displacement of point 2 (mm)	Maximum displacement of point 3 (mm)	Maximum displacement of point 4 (mm)	Maximum displacement of point 5 (mm)
1#	0.5344	0.3005	0.5549	0.5453	0.04163
2#	2.632	2.075	0.941	0	0
3#	3.9832	3.1793	2.471	0	0
4#	4.048	4.872	4.869	0	0

According to the corresponding analysis of deformation evolution and interlayer sliding displacement evolution, it can be concluded that: Firstly, in the linear loading stage, the deformation concentration occurs near the end of the roadway, and the deformation is in a stable evolution state at the end, away from the roadway. Secondly, in the stage of sub-instability, with the relative sliding displacement between layers in the end area of the roadway, the load of weak rock redistributes and the deformation concentration area is transferred to the direction away from the end of the roadway, and the deformation is characterised by fluctuation. With the increase of sliding displacement, the amplitude of deformation fluctuation increases. Thirdly, with the difference of initial interlayer shear force, the maximum value of damage sliding displacement is different. Generally speaking, the greater the initial shear stress, the greater the interlayer sliding displacement.

Through the above research on the evolution characteristics of normal strain field in the  $X$  direction in the observation area of weak layer, boundary shear strain evolution characteristics and interlayer interface friction sliding characteristics, the occurrence mechanism is analysed as follows: with the increase of load, stress concentration occurs around the roadway. As a result of stress concentration, the surrounding rock of the roadway gradually evolves from an elastic to plastic deformation state. Plastic deformation causes volume expansion of surrounding rock. Due to the constraint of interlayer shear force, the expansive rock mass extrudes the deep surrounding rock and forms the extrusion deformation area. As the deformation of expansive rock mass continues to increase, the constraint of interlayer shear force decreases. The expansive rock mass slips towards the roadway, and the stress concentration area of rock mass is transferred to the surrounding rock far away from the roadway ends. This leads to the re-formation of the stress concentration area in the deep part of surrounding rock and the emergence of the new tensile surrounding rock. Therefore, the whole surrounding rock of the roadway forms an alternating area of tension-compression-tension deformation.

According to the description of on-site monitoring results of the roadway zonal fracturing project in research [20]: (1) After roadway driving, the surrounding rock is displaced to the free face, and the relaxation area with obvious deformation is produced in the range of 0-2.5 m. (2) There is a compression zone in the depth range of 2.5-6 m of the surrounding rock. (3) In the process of continuous adjustment of surrounding rock stress, in the 6-9 m section, the surrounding rock gradually changes from the initial compression state to the later relaxation state. (4) In the section of 9-12 m, the surrounding rock gradually changed from the initial relaxation state to the

later compression state. Its main characteristics are that the radial strain value of the surrounding rock changes with time, and the relaxation zone and compaction zone appear alternately. According to the experimental study in this paper, it is considered that the relaxation zone and compaction zone of surrounding rock of roadway are mainly due to the compression-shear load between strata. With the action of interlayer normal stress, the rock transforms from elastic to plastic deformation, which produces expansion and forms a relaxation area. For another, the existence of interlayer shear force restricts the expansion of surrounding rock towards the roadway, and the expanding rock mass squeezes the deep rock mass of surrounding rock to form a compact area. When the surrounding rock slides relatively along the interlayer, the stress is redistributed and transmitted to the deep part of confining pressure, forming the characteristic of alternating tension and compression.

In addition, according to the continuous characteristics of deformation, the alternating phenomenon of tension and compression zones is in the intermediate stage of static deformation and dynamic damage of rock.

### 3.3. Study on dynamic characteristics of deformation and damage of weak rock structure

According to the above-mentioned sliding displacement evolution and the dynamic phenomenon reflected by the final model damage, the dynamic characteristics of deformation and damage of weak rock structure are studied. In the whole process, the Digital Speckle Correlation method is used to analyse the acceleration of each monitoring point based on the displacement analysis of the five monitoring points.

Fig. 12 shows the acceleration evolution curve of the corresponding position of monitoring point 1 in the whole loading process. It can be seen from the figure that in the linear loading stage, the sliding acceleration of monitoring point 1 is 0. At the peak load stage, monitoring point 1

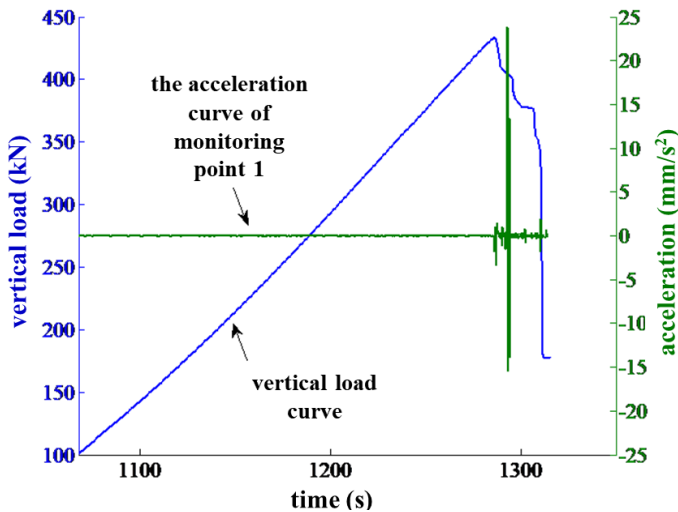


Fig. 12. The acceleration evolution curve of monitoring point 1 in loading process

slips and generates acceleration. The acceleration suddenly increases and reaches the maximum value in the sub-instability stage. In the loading instability stage, the acceleration of monitoring point 1 suddenly increases again.

Fig. 13 shows the acceleration evolution curve of five monitoring points of the model in the whole loading process. According to the comparative analysis of the time and magnitude of acceleration at five monitoring points in the figure, at the peak time of loading, monitoring points 1-3 slip and produce an acceleration, while monitoring points 4 and 5 do not slip at this time, and the acceleration is 0. In the sub-instability stage, the acceleration of monitoring points 1-3 suddenly increases and reaches the maximum value. In the loading instability stage, monitoring points 1-5 slide and accelerate.

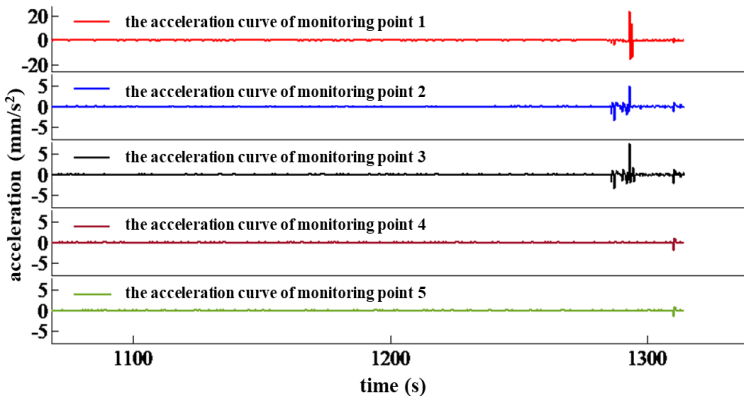


Fig. 13. The acceleration evolution curve of monitoring points in loading process

Table 3 gives the maximum acceleration value table of four groups of model experiments corresponding to five monitoring points in the sub-instability stage. It can be seen from the table that with the increase of initial shear stress, the magnitude of acceleration increases, and the dynamic characteristics become more apparent.

TABLE 3

Maximum acceleration values of measuring points in the experiment

Experiment serial number	1#	2#	3#	4#
Maximum acceleration at point 1 (mm/s <sup>2</sup> )	1.412	5.664	7.575	23.88
Maximum acceleration at point 2 (mm/s <sup>2</sup> )	1.341	3.751	1.633	5.125
Maximum acceleration at point 3 (mm/s <sup>2</sup> )	2.539	1.427	2.45	7.682
Maximum acceleration at point 4 (mm/s <sup>2</sup> )	2.306	0	0	0
Maximum acceleration at point 5 (mm/s <sup>2</sup> )	1.482	0	0	0

According to the analysis of deformation dynamic characteristics of weak rock structure, it can be concluded that: (1) When the load reaches the peak value, the weak rock damage area slides relatively along the interlayer, resulting in acceleration. (2) According to the state of static and dynamic mechanics, the deformation evolution before peak can be classified as a static process (before the peak). Zonal fracturing can be classified as the transition stage from static process to slow dynamic process (maximum acceleration from peak to the sub-instability stage), and rockburst instability can be classified as a high-speed dynamic process (maximum acceleration to instability). (3) As the initial shear stress increases, the magnitude of acceleration increases, and the dynamic characteristics become more apparent.

According to the description of rockburst mechanism in research [7]: (1) The rockburst is closely related to the structure of coal and rock strata, and the structural factors of them (with weak surface and layered structure easily causing abrupt sliding) are one of the main factors causing a rockburst. (2) From this, a three-factor mechanism model is obtained. That is, the internal factors are coal and rock impact tendency, force source factors (high-stress concentration or high deformation energy stored in external dynamic disturbance) and structural factors. The experimental research and analysis in this paper show that: First of all, due to the existence of weak layers in coal and rock mass, under the action of compression-shear load, local fracture, damage, instability and sliding of roadway surrounding rock will be caused, which is the mechanical reason for a rockburst. Secondly, even if the coal rock mass does not have the condition of impact tendency, under stress load of the horizontal direction, distribution of large shear stress is formed between layers, and the dynamic damage of the rockburst may occur. Thirdly, coal and rock mass must have a high degree of deformation concentration and enough stored elastic energy.

## 4. Conclusions

1. The experimental study of different compression-shear load models shows that the peak load of model damage tends to decrease with the increase of interlayer shear stress. With the increase of initial shear stress, the magnitude of interlayer sliding displacement increases.
2. The relaxation zone and compaction zone of the surrounding rock of roadway are mainly due to the compression-shear load between strata. With the action of interlayer normal stress, the rock transforms from elastic to plastic deformation, which produces expansion and forms a relaxation area. For another, the existence of interlayer shear force restricts the expansion of surrounding rock towards the roadway, and the expanding rock mass squeezes the deep rock mass of surrounding rock to form a compact area. When the surrounding rock slides relatively along the interlayer, the stress is redistributed and transmitted to the deep part of confining pressure, forming the characteristic of alternating tension and compression.
3. According to the state of static and dynamic mechanics, the deformation evolution before the peak can be classified as a static process (before the peak). Zonal fracturing can be classified as the transition stage from static process to slow dynamic process (maximum acceleration from peak to the sub-instability stage), and the rockburst instability can be classified as a high-speed dynamic process (maximum acceleration to instability).

4. Due to the existence of weak layers in coal and rock mass, under the action of compression-shear load, local fracture, damage, instability and sliding of roadway surrounding rock will be caused, which is the mechanical reason for a rockburst. Next, even if the coal rock mass does not have the condition of impact tendency, under stress load of the horizontal direction, distribution of large shear stress is formed between layers, and the dynamic damage of the rockburst may occur.

### Data Availability

The data used to support the findings of this study are included within the article.

### Disclosure statement

No potential conflict of interest was reported by the authors.

### Founding

This work was supported by the National Natural Science Foundation of China (no. 51474013 and 51774015).

### References

- [1] H. Lippman, The Mechanics of “Protruding” in Coal Mine: Discussion on The Violent Deformation on Both Sides of The Channel in Coal Seam [J], *Advances in Mechanics* **19** (2), 100-113+59 (1989). DOI: <https://doi.org/10.6052/1000-0992-1989-1-j1989-011>
- [2] H.T. Li, J. Liu, S.K. Zhao, L.S. Cai, Q.X. Qi, L.H. Kong, Experimental Study on The Development Mechanism of Coal Bump Considering The Clamping Effect of Roof and Floor [J], *Journal of China Coal Society* **43** (11), 2951-2958 (2018). DOI: CNKI:SUN:MTXB.0.2018-11-001
- [3] M.V. Kurlenya, V.N. Oparin, V.I. Vostrikov, Effect of Anomalously Low Friction in Block Media [J], *Journal of Applied Mechanics & Technical Physics* **40** (6), 1116-1120 (1999). DOI: <https://doi.org/10.1007/BF02469182>
- [4] L.M. Dou, H. He, J. He, Z.Y. Wang, New Method of Rock Burst Risk Assessment Using Relative Stress Concentration Factor Superposition [J], *Journal of China Coal Society* **43** (2), 327-332 (2018). DOI: CNKI:SUN:MTXB.0.2018-02-004
- [5] L.P. Li, W.J. Li, Y.S. Pan, Influence of Impact Disturbance on Anomalously Low Friction Rock Bursts [J], *Chinese Journal of Rock Mechanics and Engineering*, **38** (1), 111-120 (2019). DOI: 10.13722/j.cnki.jrme.2018.0922
- [6] L.Y. Pan, H.Z. Yang, Dilatancy Theory for Identification of Premonitory Information of Rock Burst [J], *Chinese Journal of Rock Mechanics and Engineering* **23** (1), 4528-4530 (2004). DOI: <https://doi.org/10.3321/j.issn:1000-6915.2004.z1.056>
- [7] Q.X. Qi, T.Q. Liu, Y.W. Shi, J.L. Lv, Mechanism of Friction Sliding Instability of Rock Burst [J], *Ground Pressure and Strata Control* **1**, 174-177+200 (1995). DOI: CNKI:SUN:KSYL.0.1995-Z1-042
- [8] Q.X. Qi, Y.W. Shi, T.Q. Liu, Mechanism of Instability Caused by Viscous Sliding in Rock Burst [J], *Journal of China Coal Society* **22** (2), 144-148 (1997). DOI: CNKI:SUN:MTXB.0.1997-02-006
- [9] Q.X. Qi, Z.Z. Gao, S. Wang, The Theory of Rock Burst Led by Structure Damage of Bedded Coal-rock Mass [J], *Coal Mining Technology* (2), 14-17+64 (1998). DOI: CNKI:SUN:MKKC.0.1998-02-004
- [10] E.I. Shemyakin, G.L. Fisenko, M.V. Kurlenya, V.N. Oparin, Y.S. Kuznetsov, Zonal Disintegration of Rocks around Underground Work, Part I: Data of In-situ Observations [J], *Journal of Mining Science* **22** (3), 157-168 (1986). DOI: <https://doi.org/10.1007/BF02500863>

- [11] E.I. Shemyakin, G.L. Fisenko, M.V. Kurlenya, V.N. Oparin, V.N. Reva, F.P. Glushikhin, M.A. Rozenbaum, E.A. Tropp, Y.S. Kuznetsov, Zonal Disintegration of Rocks around Underground Work, Part II: Rock Fracture Simulated in Equivalent Materials [J], *Journal of Mining Science* **22** (4), 223-232 (1986). DOI: <https://doi.org/10.1007/BF02500845>
- [12] E.I. Shemyakin, G.L. Fisenko, M.V. Kurlenya, V.N. Oparin, Y.S. Kuznetsov, Zonal Disintegration of Rocks around Underground Workings, Part III: Theoretical Concepts [J], *Journal of Mining Science* **23** (1), 1-6 (1987). DOI: <https://doi.org/10.1007/BF02534034>
- [13] E.I. Shemyakin, M.V. Kurlenya, V.N. Oparin, V.N. Reva, F.P. Glushikhin, E.A. Tropp, Zonal Disintegration of Rocks around Underground Workings, Part IV: Practical Applications [J], *Journal of Mining Science* **25** (4), 297-302 (1989). DOI: <https://doi.org/10.1007/BF02528546>
- [14] W.Q. Guo, S.P. Ma, Y.J. Kang, Q.W. Ma, Virtual Extensometer Based on Digital Speckle Correlation Method and Its Application to Deformation Field Evolution of Rock Specimen [J], *Rock and Soil Mechanics* **32** (10), 3196-3200 (2011). DOI: <https://doi.org/10.16285/j.rsm.2011.10.030>
- [15] X.T. Zhang, Q.Y. Zhang, W. Xiang, Q. Gao, S.B. Yuan, C. Wang, Model Test Study of Zonal Disintegration in Deep Layered Jointed Rock Mass [J], *Rock and Soil Mechanics* **35** (8), 2247-2254 (2014). DOI: CNKI:SUN:YTLX.0.2014-08-018
- [16] Y. Xu, P. Yuan, Model Test of Zonal Disintegration in Deep Rock under Blasting Load [J], *Chinese Journal of Rock Mechanics and Engineering* **34** (S2), 3844-3851 (2015). DOI: CNKI:SUN:YSLX.0.2015-S2-027
- [17] Y.M. Song, Z.X. Zhao, L.L. Deng, J.N. Wu, Deformation Field and Acoustic Emission Characteristics of Marble during Sub-instability Stage [J], *Journal of Liaoning Technical University* **37** (3), 541-546 (2018). DOI: CNKI:SUN:FXY.0.2018-03-016
- [18] Y.S. Pan, K.X. Wang, Pendulum-type Waves Theory on The Mechanism of Anomalously Low Friction between Rock Masses [J], *Seismology and Geology* **36** (3), 833-844 (2014). DOI: <https://doi.org/10.3969/j.issn.0253-4967.2014.03.022>
- [19] Y.S. Pan, Y.H. Xiao, Z.H. Li, K.X. Wang, Study of Roadway Support Theory of Rock Burst in Coal Mine and Its Application [J], *Journal of China Coal Society* **39** (2), 222-228 (2014). DOI: <https://doi.org/10.13225/j.cnki.jccs.2013.2015>
- [20] Z.L. Fang, Study on The Ground Pressure and Control Method for Openings in Soft and Broken Rocks in Jin Chuon Mine No. 2 [J], *Journal of Beijing Iron and Steel Institute* (1), 1-20 (1984). DOI: CNKI:SUN:BJKD.0.1984-01-000